Section: Research Paper

Powell-Erying-Nanofluid flow numerical solutions towards a stretched porous sheet with the influence of double diffusion and Magnetic field

R. S. DurgaRao[*], R. Vijaya Kumar[1] and V. Vasudeva Murthy[2]

[*] Department of Mathematics, Vishnu Institute of Technology, Bhimavaram, West Godavari (Dt), 534201,
Andhra Pradesh, India. durgarao.r@vishnu.edu.in

[1] Mathematics Section, FEAT, Annamalai University, Tamilnadu, India
Department of Mathematics, Periyar Arts College,Cuddalore, Tamilnadu, India,

[2] Department of Mathematics, S. R. K. R. Engineering College, Bhimavaram, West Godavari (Dt), 534201,
Andhra Pradesh, India.

[1]Corresponding author Email address: rathirath_vijiyahoo.co.in

Abstract: This article tries to explain how thermal diffusion and heat diffusion affect on the flow of magnetohydrodynamic (MHD) Powell-Erying nanofluids across a stretched surface filled with porous material when thermal and mass Biot numbers are present. Due to the nanoparticles and Powell-Erying fluid, thermophoresis and Brownian motion are brought into play. With right factors, the basic nonlinear equations of motion, energy, and concentration can be turned into formulas with no units. The The Runge-Kutta method is used in conjunction utilising the Shooting Technique to find the math answers. There are graphs that show how the combined factors affect speed, temperature, and the number of nanoparticles. The numbers of coefficient of skin friction, the area Nusselt numbers, and the Sherwood numbers are used to do calculations and studies.

Keywords: Powell-Erying fluid; Magnetic field; Nanofluid; Double diffusion (Soret & Dufour); Porous medium; Stretching sheet; Numerical Solutions;

Nomenclature

List of Symbols

u, v : Velocity Components in the x and y directions, respectively (m/s)

x, y : Calculated Cartesian coordinates toward the stretching sheet(m)

f : Nom dimensional Stream function

f' : Fluid's Velocity (m/s)

Pr : Prandtl number

T : Fluid's Temperature (K)

C : Volume concentration of Fluid nanoparticle (mol / m^3)

C_∞ : Dimensional ambient volume fraction (mol / m^3)

C_f : Dimensional concentration of hot fluid (mol / m^3)

T_f : Dimensional temperature of hot fluid

B_o : Uniform magnetic field (Tesla)

M : Magnetic field parameter

T_∞ : Fluid temperature away from the stretched sheet (K)

Cf : Skin-friction coefficient (s^{-1})

Nb : Parameter of Brownian motion

u_w : Fluid's Stretching velocity (m/s)

Nu : Nusselt number(or)

heat transfer coefficient rate

Nt : Thermophoresis parameter

C^* : Material constant

Le : Lewis number

q_w : Heat flux coefficient

q_m : Coefficient of Mass flux

C_p : Nano particles Specific heat capacity Nano particles (J / kg / K)

D_B : Coefficient Brownian diffusion

D_T : Coefficient of Thermophoresis diffusion (m^2 / s)

Sh : Sherwood number(or) Mass transfer coefficient rate

K : Parameter of Permeability (m^{-1})

k_1 : Permeability of porous medium (m^{-1})

a : Positive real number

Re_x : Reynold's number

Du : Dufour number

Sr : Soret number

C_s : Susceptibility Concentration

K_T : Ratio of Thermal diffusion ratio

D_m : Solutal diffusivity of the medium

T_m : Fluid Mean temperature

Re_x : Reynold's number

R : Thermal radiation parameter

q_r : Radiative heat flux

K^* : Coefficient of Mean absorption

n : stretching sheet ‘s Parameter

Greek symbols

η : Variable of dimensionless similarity (m)

θ : Temperature in Non-dimensional (K)

ϕ : Nanoparticle concentration in Non-Dimensional (mol / m^3)

α_m : Thermal diffusivity, (m^2 / s)

ν : Kinematic viscosity, (m^2 / s)

σ : Electrical conductivity

ρ_f : Fluid’s Density , (kg / m^3)

μ : Fluid dynamic viscosity,

κ : Fluid Thermal conductivity (W / (m·K))

τ_w : Shear stress

δ : Biot thermal number

ζ : Mass Biot number

β_1 : Non-uniform heat transfer coefficient

λ_1 : Non-uniform mass transfer coefficient

σ^* : Stefan Boltzmann constant

β : parameter of Powell-Eyring fluid

λ : Powell-Eyring fluid parameter

χ : Material constant

Superscript:

$'$: Derivative w.r.t η

Subscripts:

f : Fluid,

w : Condition on the sheet,

∞ : Ambient Conditions.

1. Introduction:

Nanoparticles are suspended in a Powell-Eyring fluid in Powell-Eyring-nanofluid flow, a kind of non-Newtonian fluid flow. Engineered fluids known as nanofluids may improve their qualities, such as thermal conductivity, heat transfer coefficient, and, viscosity, by floating nanoparticles in a base fluid. A Powell-Eyring fluid's non-Newtonian behaviour may be further altered by nanoparticles, changing the flow properties. For instance, the yield stress-the shear stress necessary to start a flow-may be increased by the presence of nanoparticles. When a fluid has to retain its stability at rest while flowing smoothly when forced to an external force, such as during pipeline gearbox, this trait may be helpful. The use of Powell-Eyring nanofluids in many industrial processes, including heat transmission, has been investigated. It has been shown that they have greater thermal conductivity than base fluids. As a consequence, heat transfer could be more effective, which might have a big impact on how successfully

different businesses use energy. To effectively employ Powell-Eyring-nanofluids in industrial settings, it is crucial to comprehend their flow behaviour. To comprehend this complicated fluid flow behaviour better, computational models and experimental experiments are being created. Powell-Eyring- flow of the nanofluid and heat transport in a concentric annulus were examined experimentally and numerically by Ali and Rashidi [1] in their research. A statistical investigation of the nanofluid Powell-Eyring flow over a stretched sheet was executed by Aziz et al. [2]. The unsteady MHD flow of Powell-Eyring nanofluid along a stretching/ shrinking a sheet with a source/sink of heat was known by Bachok et al. [3]. The MHD nanofluid flow of Powell-Eyring across a moving surface was heated by radiation and a chemical reaction occurred it is investigated by Bora et al. [4]. In an exploratory flow of Powell-Eyring nanofluid research in a rectangular microchannel, Ghadimi et al. [5]. nanofluid Powell-Eyring flow in a microchannel T-junction was researched by Ghadimi et al. [6]. Entropy formation was investigated by Jamil et al. [7] in Powell-Eyring flow of nanofluid on a spinning disc with regard to dissipation of viscous fluid. Within a channel with a wall -mounted obstruction, Kamali et al. carried out a numerical process examination of the heat transfer and turbulent Powell-Eyring nanofluid flow. [8]. Karami et al. [9] investigated the Powell-Eyring heat transmission and nanofluid flow in a rotating system using numerical methods. In a vertical tube with a moving wall, Karimipour et al. [10] examined the magnetohydrodynamic Powell-Eyring flow of nanofluid. In a lid-driven square, Powell-Eyring nanofluid flow and heat transfer were computed by Khoddadi and Rashidi. [11]. A theoretical examination of the nanofluid Powell-Eyring flow of in a microchannel was carried out by Li et al. [12]. Simulations based on numbers were performed by Liu and Zhang [13] to investigate the nanofluid Powell-Eyring 's flow properties in a curved microchannel. Entropy analysis in nanofluid Powell-Eyring flow of with heat Convective boundary and radiation conditions was observed by Malik et al. [14]. Powell-Eyring is the flow of nanofluid on a Convective boundary conditions on a stretched sheet was studied by Mishra and Mehta [15]. Nouri-Borujerdi et al. [16] conducted an experiment investigation and a CFD simulation Transfer of heat and fluid flow features of the nanofluid Powell-Eyring. In the existence of heat radiation, Oztop et al.'s [17] examination of the nanofluid flow across a stretched sheet had convective boundary conditions. carried out. Research on Powell-Eyring nanofluid flow in a rotating curved channel for heat transfer analysis is done by Rashidi and Karimipour [18]. The flow of nanofluids and heat transmission in a conduit partly stuffed with porous mediam are examined in Rashidi and Rashidi [19]. Rashidi et al. [20] investigated magnetic field flow effect vertical porous channel, whereas Rashidi et al. [21] investigated passage of a nanofluid via a porous tube moving wall Powell-Eyring heat transfer and nanofluid flow were thoroughly covered by Rezaei et al. [22], who also included models and applications. Sahoo et al. [23] conducted a nanofluid flow of Powell-Eyring numerical analysis in a T-junction microchannel, whereas Sahoo et al. [24] observed the flow in a rectangular microchannel. nanofluid flow of the Powell-Eyring was described by the authors of the paper by Saqib et al. [25] using the Caputo-Fabrizio fractional derivative. A lid-driven cavity's mixed convection Powell-Eyring nanofluid flow was quantitatively known by Sattari et al. [26]. Through the use of a conduit, Seetharamu and Sundararajan [27] investigated and modelled the Powell-Eyring flow of nanofluid. heat transfer and flow of Powell-Eyring nanofluid were the subjects of a review of the literature by Sharma and Bhargava [28]. In a hollow with wavy walls, Powell-Eyring nanofluid flow and heat transfer were numerically analysed by Sheikholeslami and Rashidi [29]. The unstable flow of convectional mixing Powell-Eyring nanofluid flow in an asymmetric a vertical channel boundary conditions was studied by Vafai and Khaledi [30]. The majority of Wang and Pop's research [31] was devoted to numerically simulating nanofluid Powell-Eyring flow across a porous stretched surface. For a Powell-Eyring nanofluid flow

circular tube under laminar flow conditions, Wang et al. [32] developed heat transfer and friction factor correlations. Single-walled carbon nanotubes have reportedly been introduced to the Powell-Eyring nanofluid to improve heat transmission, according to Wong and Leon [33]. The edited book by Wongwises and Hayat [34] discusses the rheology, heat transmission, and engineering applications of the Powell-Eyring nanofluid dynamics. Heat radiation's influence based on the Powell-Eyring nanofluid flow in a tube with an expanding or contracting wall was verified by Yu et al. [35]. The convective heat transfer brought on by nanofluid flow of Powell-Eyring in a porous channel was the subject of Zaki et al.'s study [36]. Powell-Eyring nanofluid flow numerical analysis in a T-shaped microchannel with expansion-contraction was done by Zhang et al. [37]. Powell-Eyring flow of nanofluid and heat transport across a stretched sheet were studied by Zheng and Zheng [38].

With the above factors in mind, we are constructing a mathematical model of nanofluid using a fluid of Powell-Eyring as the working fluid. Consideration is given to a hydromagnetic flow in relation to a porous medium, heat diffusion, and thermo diffusion. The thermal and mass Biot numbers are enforced at the sheet's edge. As a result of nonlinear partial differential equations, the resulting expressions are interconnected and extraordinarily intricate. Using the Runge-Kutta method these equations are analysed and discharge technique. Utilising graphs and numerical standards to display and illustrate the results.

2. Flow Governing Equations

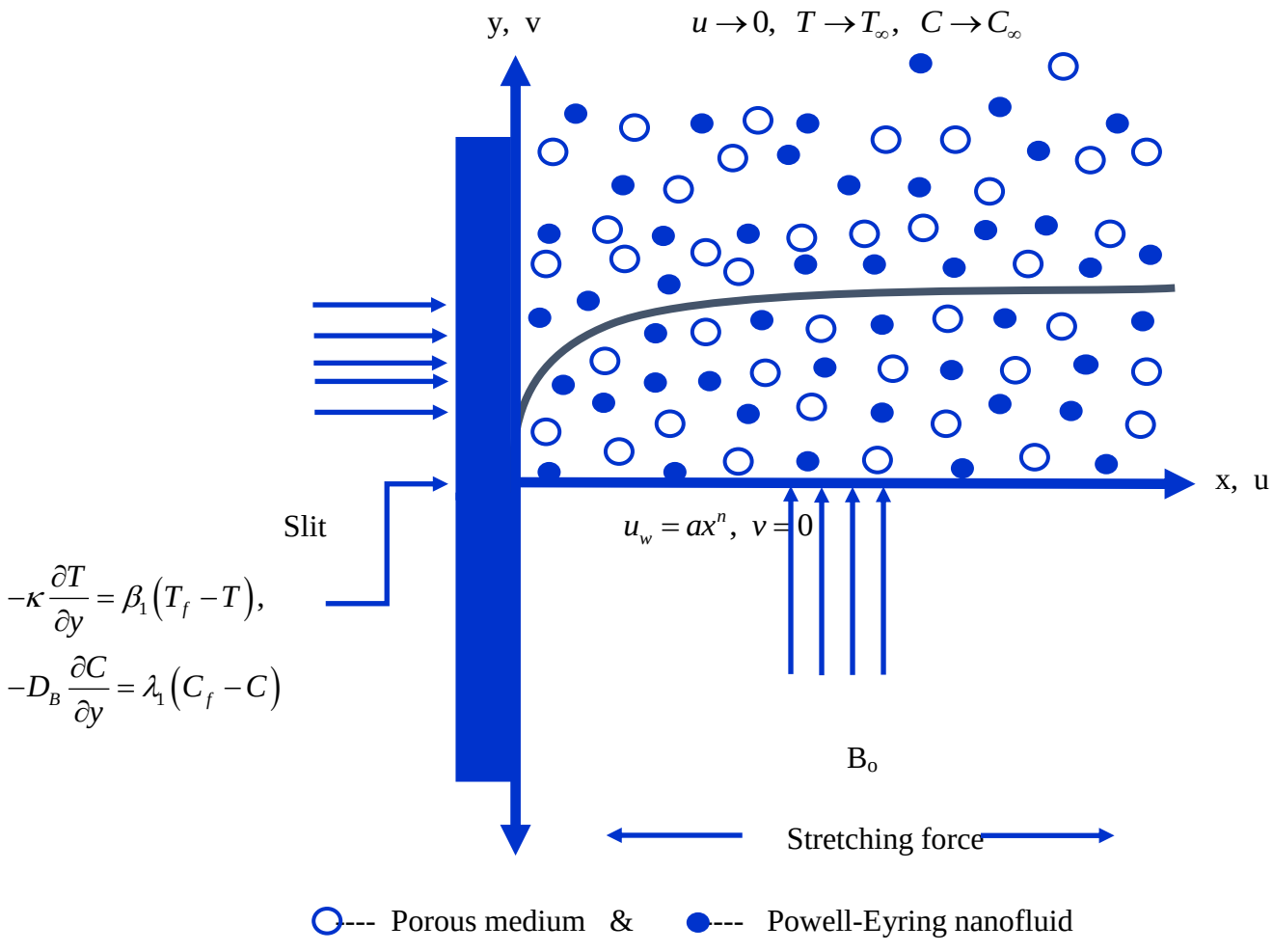

Fig. 1.: Geometry representation of the Powell-Eyring nanofluid

Brownian motion, thermal diffusion (Soret), diffusion thermo, thermal convective boundary condition, magnetic field, fluid flow of non-Newtonian Powell-Eyring in two-dimensional, and steady flow approaching a non-linear stretched sheet packed with porous medium are all investigated. The geometry flow of our experiment is shown in Fig. 1. Regarding this evaluation, the following premises are made:

i. The coordinate axes are chosen to be parallel to and perpendicular to the flow direction, respectively.
ii. The assumption is that, at the boundary conditions for convective heat and mass is enforced.
iii. The sheet surface is heated with a hot fluid with temperature T_f and concentration C_f, resulting in coefficients of heat and mass transfer of β_1 and λ_1, respectively.
iv. Along x-axis with a velocity $u_w = ax^n$ the plate is stretched, where stretching parameter $a > 0$.
v. The thermophoresis and Brownian motion effects are taken into account in both energy and concentration equations.
vi. Neglecting Impacts of Hall current and electric field .
vii. Small magnetic fields coefficient of Reynolds do not affect the induced magnetic field..
viii. Via non-uniform magnetic field B (x) fluid is taken electrically conducted in direction of y-axis
ix. Because of the induced The magnetic field is considered modest since the magnetic Reynolds number is assumed to be low
x. The impacts of Joule heating, viscous dissipation and body forces to be neglected.
xi. The Dufour and Soret effects are considered in energy and concentration equations respectively.
xii. In concentration equation
xiii. The impact of chemical reaction of first order is neglected.

Based on the assumptions stated above, the basic equations governing flow for Powell-Erying nanofluid flow are:

Continuity Equation:

$$\frac{\partial u}{\partial x}+\frac{\partial v}{\partial y}=0, \tag{1}$$

Momentum Equation :

$$u\frac{\partial u}{\partial x}+v\frac{\partial u}{\partial y}=\left(\nu+\frac{1}{\rho_f \chi C^*}\right)\frac{\partial^2 u}{\partial y^2}-\frac{1}{2\rho_f \chi C^{*3}}\left(\frac{\partial u}{\partial y}\right)^2\frac{\partial^2 u}{\partial y^2}-\left(\frac{\sigma B^2(x)}{\rho_f}\right)u-\nu\left(\frac{u}{k_1}\right), \tag{2}$$

The Equation of thermal energy:

$$u\frac{\partial T}{\partial x}+v\frac{\partial T}{\partial y}=\alpha_m\frac{\partial^2 T}{\partial y^2}+\frac{(\rho C)_p}{(\rho C)_f}\left\{D_B\left(\frac{\partial C}{\partial y}\frac{\partial T}{\partial y}\right)+\frac{D_T}{T_\infty}\left(\frac{\partial T}{\partial y}\right)^2\right\}+\frac{D_m K_T}{C_s C_p}\left(\frac{\partial^2 C}{\partial y^2}\right)-\frac{1}{(\rho C)_f}\left(\frac{\partial q_r}{\partial y}\right), \tag{3}$$

The Equation of species nanoparticle volume concentration:

$$u\frac{\partial C}{\partial x}+v\frac{\partial C}{\partial y}=D_B\frac{\partial^2 C}{\partial y^2}+\frac{D_T}{T_\infty}\frac{\partial^2 T}{\partial y^2}+\frac{D_m K_T}{T_m}\left(\frac{\partial^2 T}{\partial y^2}\right), \tag{4}$$

for this flow the conditions of boundary are

$$\left.\begin{array}{l} u = u_w(x) = ax,\ v = 0,\ -\kappa\dfrac{\partial T}{\partial y} = \beta_1\left(T_f - T\right),\ -D_B\dfrac{\partial C}{\partial y} = \lambda_1\left(C_f - C\right)\ at\ \ y = 0 \\ u \to 0,\ T \to T_\infty,\ C \to C_\infty\ \ as\ \ y \to \infty \end{array}\right\} \tag{5}$$

By using Rosseland approximation the radiative heat flux q_r is defined as

$$q_r = -\frac{4\sigma^*}{3K^*}\left(\frac{\partial T^4}{\partial y}\right) \tag{6}$$

We suppose that within the flow the temperature variations is such that T^4 can be expressed as a dependent temperature linear function. This is performed by broadening T^4 in a Taylor series concerning free stream temperature T_∞ as follows:

$$T^4 = T_\infty^4 + 4T_\infty^3\left(T - T_\infty\right) + 6T_\infty^2\left(T - T_\infty\right)^2 + \ldots\ldots\ldots \tag{7}$$

we get after neglecting higher-order words beyond the first degree term in $\left(T - T_\infty\right)$ the preceding equation, $T^4 \cong 4T_\infty^3 T - 3T_\infty^4$

(8)

by applying Eq. (8) in Eq. (6), we get

$$q_r = -\frac{16T_\infty^3\sigma^*}{3K^*}\left(\frac{\partial T}{\partial y}\right) \tag{9}$$

it can be written as by using(9), then Eq. (3)

$$u\frac{\partial T}{\partial x} + v\frac{\partial T}{\partial y} = \alpha_m\frac{\partial^2 T}{\partial y^2} + \frac{\left(\rho C\right)_p}{\left(\rho C\right)_f}\left\{D_B\left(\frac{\partial C}{\partial y}\frac{\partial T}{\partial y}\right) + \frac{D_T}{T_\infty}\left(\frac{\partial T}{\partial y}\right)^2\right\} + \frac{D_m K_T}{C_s C_p}\left(\frac{\partial^2 C}{\partial y^2}\right) + \frac{1}{\rho C_p}\left(\frac{16T_\infty^3\sigma^*}{3K^*}\right)\left(\frac{\partial^2 T}{\partial y^2}\right),$$

(10)

The following similarity transformation can be utilized to get ordinary differential equations as governing equations.

$$\left.\begin{array}{l} u = ax^n f'(\eta),\ v = -\sqrt{\dfrac{a\nu\left(n+1\right)}{2}}x^{\frac{n-1}{2}}\left\{f(\eta) + \left(\dfrac{n-1}{n+1}\right)\eta f'(\eta)\right\}, \\ \eta = y\sqrt{\dfrac{a\left(n+1\right)}{2\nu}}x^{\frac{n-1}{2}},\ \ \theta = \dfrac{T - T_\infty}{T_f - T_\infty},\ \ \phi = \dfrac{C - C_\infty}{C_f - C_\infty} \end{array}\right\}, \tag{11}$$

Using the similarity transformations (11), the basic governing equations (2), (4) and (10) together using boundary conditions (5) can take the following forms:

$$\left(1+\beta\right)f''' - \left(\frac{n+1}{2}\right)\beta\lambda f''f''^2 + ff'' - \left(\frac{2n}{n+1}\right)\left(f'^2\right) - \left(M + K\right)f' = 0, \tag{12}$$

$$\left(1 + \frac{4R}{3}\right)\theta'' + \Pr\ f\theta' + \Pr\ Nb\theta'\phi' + \Pr\ Nt\theta'^2 + \Pr\ Du\phi'' = 0, \tag{13}$$

$$Nb\phi'' + NbLe\Pr\ f\phi' + Nt\theta'' + SrNb\theta'' = 0, \tag{14}$$

the associated boundary conditions (5) become

$$\left.\begin{array}{l} f'(0) = 1,\ f(0) = 0,\ \theta'(0) = -\delta\left(1 - \theta(0)\right),\ \phi'(0) = -\zeta\left(1 - \phi(0)\right), \\ f'(\infty) \to 0,\ \theta(\infty) \to 0,\ \phi(\infty) \to 0 \end{array}\right\}, \tag{15}$$

where the physical factors at stake are specified as

$$\left.\begin{aligned}
&\beta=\frac{1}{\mu\chi C^{*}},\ \lambda=\frac{u_w^3}{2\nu x C^{*2}},\ M=\frac{2\sigma B_o^2}{\rho_f a\left(n+1\right)},\ K=\frac{\nu}{ak_1},\ \mathrm{Pr}=\frac{\nu}{\alpha_m},\ \zeta=\frac{\lambda_1}{D_B}\sqrt{\frac{2\nu}{a\left(n+1\right)}},\\
&Nb=\frac{\left(\rho C\right)_p D_B\left(C_f-C_\infty\right)}{\nu\left(\rho C\right)_f},\ Nt=\frac{\left(\rho C\right)_p D_T\left(T_f-T_\infty\right)}{\nu\left(\rho C\right)_f T_\infty},\ Le=\frac{\nu}{D_B},\ R=\frac{4T_\infty^3\sigma^{*}}{K^{*}\kappa},\\
&Sr=\frac{D_m K_T\left(T_f-T_\infty\right)}{T_m\nu\left(C_f-C_\infty\right)},\ Du=\frac{D_m K_T\left(C_f-C_\infty\right)}{C_s C_p\nu\left(T-T_\infty\right)},\ \delta=\frac{\beta_1}{\kappa}\sqrt{\frac{2\nu}{a\left(n+1\right)}},\ \mathrm{Re}_x=\frac{u_w x}{\nu}
\end{aligned}\right\},\tag{16}$$

The Skin-friction coefficient (Cf), local Nusselt number (Nu) and local Sherwood number (Sh), physical quantities are defined as

$$Cf=C_f\left(\sqrt{\mathrm{Re}_x}\right)=\frac{\tau_w}{\rho u_w^2}=\sqrt{\frac{n+1}{2}}\left\{\left(1+\beta\right)f''\left(0\right)-\frac{1}{3}\left(\frac{n+1}{2}\right)\beta\lambda f''^{3}\left(0\right)\right\}\tag{17}$$

$$Nu=\frac{xq_w}{\kappa\left(T_f-T_\infty\right)}=-\frac{x\left(\frac{\partial T}{\partial y}+\frac{\partial q_r}{\partial y}\right)_{y=0}}{\kappa\left(T_f-T_\infty\right)}\Rightarrow Nu=-\sqrt{\frac{n+1}{2}}\left(1+\frac{4R}{3}\right)\left(\sqrt{\mathrm{Re}_x}\right)\theta'\left(0\right)\tag{18}$$

$$Sh_x=\frac{xq_m}{D_B\left(C_f-C_\infty\right)}=-\frac{D_B\left(\frac{\partial C}{\partial y}\right)_{y=0}}{\left(C_f-C_\infty\right)}\Rightarrow Sh=Sh_x\left(\mathrm{Re}_x\right)^{\frac{-1}{2}}=-\sqrt{\frac{n+1}{2}}\phi'\left(0\right)\tag{19}$$

3. Method of Solution by Runge-Kutta method:

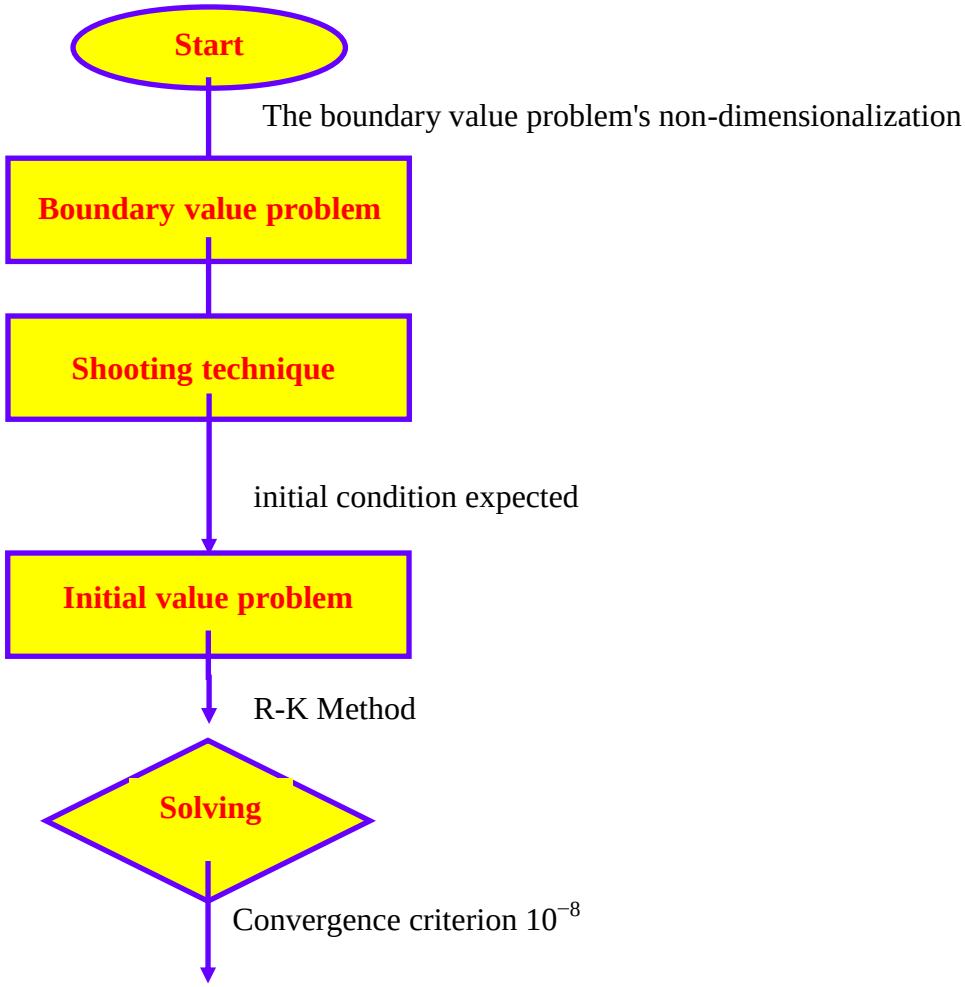

Fig. 2.: Flow diagram of the numerical procedure

In the event of a complete set of Eqs. (12)-(14), an accurate solution does not appear to be achievable. This is owing to the nonlinear character of (12)-(14), with appropriate boundary conditions supplied in Eq. (15), as well as the necessity for numerical solutions to the issue: Transformations of similarity are used in order to convert the controlling partial derivible equations into a collection ordinary differential equations that are non-linear that may be solved numerically. The shooting strategy is combined by employing a fourth-order Runge-Kutta approach numerically fix the limit value problem that results. Decomposing the transformation of a set of nonlinear differential equations into a collection of first-order derivable equations results in a collection of differential equations first-order. As shown in the diagram, the coupled equations of ordinary differential type (12)–(14) have been simplified for seven unknowns from a set of seven simultaneous equations. The linked ordinary differential equations (12)-(14) are of third order in f (η) and second order θ (η) and ϕ (η), respectively, and have been reduced to seven concurrent equations for seven unknowns. To solve this set of equations numerically, use the Runge-Kutta technique, herein, the solutions require seven beginning conditions in total, but only two starting conditions in f (η) each of which has one beginning condition θ (η) and ϕ (η) are known. On the other hand the values of $f'(\eta)$, θ (η) and ϕ (η) are known at $\eta \to \infty$. These end conditions are utilised to

generate previously unknown starting circumstances at η = 0 with shooting technique method. The most crucial step in this strategy is to select a suitable finite value of η_∞. To calculate the value of η_∞ We begin with a guess value and work our way through the boundary value issue with Eqs. (12)-(14) to obtain $f''(0)$, $\theta'(0)$ and $\phi'(0)$. The procedure of solution is repeated with a larger value of η_∞ until two consecutive values of $f''(0)$, $\theta'(0)$ and $\phi'(0)$ immediately following the required significant digit. The last number η_∞ is considered as the limit's finite value η_∞ for the specific set of physical The influencing factors for velocity, temperature, and concentration are f (η), θ (η) and ϕ (η) in the boundary layer. After obtaining all of the initial conditions, we use the fourth order Runge-Kutta integration strategy to solve the set of simultaneous equations. Depending on the physical conditions driving the flow, the value of $\eta_\infty$is set to 10 to ensure that no numerical oscillation occurs. As a result, the linked third and second order boundary value problem of in f (η), in θ (η) and ϕ (η) respectively has been decreased to a set of As follows, for seven unknowns of seven first-order simultaneous equations:

$$\left.\begin{aligned} f' = p \Rightarrow f'' = p' = q \Rightarrow f''' = p'' = q' \Rightarrow q' &= \frac{Mp + Kp - fq + \left(\frac{2n}{n+1}\right)p^2}{\left\{(1+\beta) - \left(\frac{n+1}{2}\right)\beta\lambda q^2\right\}} \\ \theta' = r \Rightarrow \theta'' = r' \text{ then } r' &= \frac{-(\Pr)\,fr - (\Pr)(Nb)\,rz - (\Pr)(Nt)\,r^2 - (\Pr)(Du)\,z'}{\left(1+\frac{4R}{3}\right)} \\ \& \\ \phi' = z \Rightarrow \phi'' = z' \text{ then } z' &= \frac{-(Le)(Nb)(\Pr)\,fz - (Nt)\,r' - (Sr)(Nb)\,r'}{Nb} \end{aligned}\right\} \quad (20)$$

and the necessary boundary conditions emerged as

$$\left.\begin{aligned} &p(0) = 1,\ f(0) = 0,\ r(0) = -\delta\left(1-\theta(0)\right),\ z(0) = -\zeta\left(1-\phi(0)\right), \\ &\&\ p(\infty) \to 0,\ \theta(\infty) \to 0,\ \phi(\infty) \to 0 \end{aligned}\right\} \quad (21)$$

The boundary value problem is initially transformed into a problem of starting value (IVP), after which investigated further. The initial value issue is then addressed by properly estimating for different permutations of the missing beginning value components using the shooting approach, which is continued until the issue is resolved. In this case for calculating purposes we used the step size h = 0.1. additionally, a 10^{-6} error tolerance is employed. The obtained material is given in the form of tables and graphs, with the principal topics addressed and thoroughly researched.

4. Program Code Validation:

Table-1: Skin-friction coefficient values were compared to Cortell's [39] published data. when K = β = λ = M = Sr = Du = 0

n	Cortell [39] Skin-friction coefficient results	Present Skin-friction coefficient results
0.00	0.627547	0.616741907983461
0.20	0.766758	0.758678229813983

0.50	0.889477	0.879967081989870
0.75	0.953786	0.949673483193904
1.00	1.000000	0.999984978463919
1.5	1.061587	1.059678679368046

Table-1 compares the outcomes of the existing findings of Skin-friction coefficient (–f"(0)) results with Cortell [39] in absence of Porous medium, Powell-Erying fluid, Thermal diffusion, Diffusion thermo and Magnetic field. From this table, the comparison reveals that the results are congruent with the published results.

5. Conclusions and Discussion:

The generated solutions in numerical profiles of velocity, temperature, and concentration are described using graphs for changes of several physical factors such as the magnetic field parameter ($M \in [0.3, 1.0]$) in this results and discussion section, Permeability parameter ($K \in [0.3, 1.0]$), Powell-Eyring fluid parameters (λ & $\beta \in [0.3, 1.0]$), Stretching sheet parameter ($n \in [0.3, 1.0]$), Prandtl number ($Pr \in [0.71, 7.0]$), Thermal radiation parameter ($R \in [0.5, 1.0]$), Parameter of Thermophoresis ($Nt \in [0.3, 1.0]$), parameter of Brownian motion ($Nb \in [0.5, 1.5]$), Thermal diffusion parameter or Soret number ($Sr \in [0.5, 2.0]$), Diffusion thermo parameter or Dufour number ($Du \in [0.5, 2.0]$), Thermal Biot number ($\delta \in [0.5, 2.0]$), Mass Biot number ($\zeta \in [0.5, 2.0]$) and Lewis number ($Le \in [0.5, 1.8]$) in Figs. 3 to 18 and followed by the calculated values in numerical of engineering amounts such as coefficient of Skin-friction (Cf), Heat transfer coefficient rate expressed in other terms of Nusselt number (Nu) and Mass transfer coefficient of rate expressed in other terms of Sherwood number (Sh) are discussed and presented in tables 2, 3 and 4. For entire graphs and tabular values, the basic values $M = 0.5$, $K = 0.3$, $\beta = 0.3$, $\lambda = 0.3$, $n = 0.3$, $Pr = 0.71$, $R = 0.5$, $Nb = 0.5$, $Nt = 0.3$, $Du = 0.5$, $Sr = 0.5$, $Le = 0.3$, $\delta = 0.5$ and $\zeta = 0.5$ are fixed. Fig. 3 demonstrates the variations of the parameter of Magnetic field (($M \in [0.3, 1.0]$)) on velocity profiles. As M rises, a drag-like resistive force is created, which is referred to as the Lorentz force. The Lorentz force retards the velocity intensity, slowing its motion. Fig. 4 illustrates the impacts of Permeability parameter ($K \in [0.3, 1.0]$), on the velocity profiles. We may extrapolate from this figure that when the parameter of porosity K grows, the profile of velocity decreases. This is because increasing K amplifies the porous layer, diminishing the momentum boundary layer thickness. Fig. 5 explores fluid variable $\beta \in [0.3, 1.0]$ effect on profiles of velocity. It is clear that bigger increases velocity and layer thickness. Physically, greater values of β show a decrease in viscosity, resulting in β an increase in velocity of fluid. Fig. 6 delineates the characteristics of $\lambda \in [0.3, 1.0]$. Fig. 7 shows the influence of the parameter of stretching that is not linear sheet ($n \in [0.3, 1.0]$), on velocity profiles. The profile of velocity for greater values of n increases, as seen in Fig. 7. This increase in non-dimensional stretching velocity is caused by a higher value of n, which causes greater deformation in the liquid. As the value of n increases, the associated momentum boundary layer becomes thicker. Fig. 8 illustrates how the Prandtl number ($Pr \in [0.71, 7.0]$) affects the temperature field ($Pr \in [0.71, 7.0]$). It has been discovered that increasing the Prandtl number Pr reduces both the field of temperature and the thickness of the thermal layer. Physically, thermal diffusivity is to blame for lower temperatures since the Prandtl number Pr is a component of it. Larger Prandtl numbers Pr result in less thermal diffusivity, which translates to a field with a lower temperature and smaller thermal layer thickness.. Fig. 9 demonstrates the varies that are seen in temperature profiles owing to an increase in the values of ($R \in$

[0.5, 1.0]). The fluid temperature rises as R rises, owing to the increased the nanofluid's conduction effect in the presence of R. As a result, greater R values suggest increased surface heat flow and, as a result, increased temperature within the boundary layer region. Fig. 10 displays the temperature field fluctuation for various Brownian motion parameter values (Nb $\in$ [0.5, 1.5]). This figure shows that raising the parameter of motion of the Brownian motion Nb resulted in an improvement in the field of temperature and its associated thickness of thermal layer. From Fig. 11, It is clearly demonstrated that utilising a bigger Brownian motion parameter (Nb $\in$ [0.5, 1.5]) produces a weaker concentration field.. Fig. 12 is drawn to demonstrate the impact of the parameter of Thermophoresis (Nt $\in$ [0.3, 1.0]), on temperature field. A greater temperature field and thickness thermal layer is represented by higher values of the thermophoresis parameter Nt. The reasoning behind this statement is that increasing Nt results in a greater thermophoretic force, which allows for deeper migration of nanoparticles in fluids further away from the surface, resulting in a larger temperature field and thickness of thermal layer. Fig. 13 shows that the higher thermophoresis parameter (Nt $\in$ [0.3, 1.0]), yield a stronger concentration field. Figs. 14 and 15, one after the other, so that you can see how the Dufour number (Du $\in$ [0.5, 2.0]), and the Soret number (Sr $\in$ [0.5, 2.0]), behave in relation to profiles of the temperature and concentration. When examining this figure, we found that increasing the value of Du led to a rise in both the temperature and the thermal layer thickness. The effect of a concentration gradient on the amount of thermal energy contained inside a liquid is physically related to Du. Similar to how increasing Sr levels improves concentration profiles, so do rising Sr values. This is because a temperature gradient enhances mass transfer from a lower to a higher concentration of the solute. Fig. 16 depicts the thermal Biot number ($\delta \in$ [0.5, 2.0]) effect , on the temperature scale. An increase δ in causes greater convection, which results in an a rise in temperature field Fig. 17 illustrates the impact of mass Biot number ($\zeta \in$ [0.5, 2.0]) on the concentration profile. Concentration profiles are a mass-increasing function the Biot number. Fig. 18 demonstrates that The concentration profile decreases as the Lewis number decreases (Le $\in$ [0.5, 1.8]). Brownian diffusivity is the physical basis for the Lewis number.. A greater Le value results in a lower Brownian diffusivity. This lower concentration field leads to a poorer Brownian diffusivity. Table-2 illustrates the Skin-friction coefficient numerical values as engineering variables such as, magnetic field parameter (M $\in$ [0.3, 1.0]), Permeability parameter (K $\in$ [0.3, 1.0]), Powell-Eyring fluid parameter (λ & $\beta \in$ [0.3, 1.0]), Stretching sheet parameter (n $\in$ [0.3, 1.0]), Prandtl number (Pr $\in$ [0.71, 7.0]), Thermal radiation parameter (R$\in$ [0.5, 1.0]), parameter of Thermophoresis (Nt $\in$ [0.3, 1.0]), parameter of Brownian motion (Nb $\in$ [0.5, 1.5]), Thermal diffusion parameter or Soret number (Sr $\in$ [0.5, 2.0]), Diffusion thermo parameter or Dufour number (Du $\in$ [0.5, 2.0]), Thermal Biot number ($\delta \in$ [0.5, 2.0]), Mass Biot number ($\zeta \in$ [0.5, 2.0]) and Lewis number (Le $\in$ [0.5, 1.8]). According to this table, the Skin-friction coefficient increases as the Powell-Eyring fluid parameters increase. ($\beta \in$ [0.3, 1.0]), Parameter of Thermal radiation (R$\in$ [0.5, 1.0]), Thermophoresis parameter (Nt $\in$ [0.3, 1.0]), parameter Brownian motion (Nb $\in$ [0.5, 1.5]), Thermal diffusion parameter or Soret number (Sr $\in$ [0.5, 2.0]), Diffusion thermo parameter or Dufour number (Du $\in$ [0.5, 2.0]), Thermal Biot number ($\delta \in$ [0.5, 2.0]), Mass Biot number ($\zeta \in$ [0.5, 2.0]), while it decreases with increasing Magnetic field parameter values (M $\in$ [0.3, 1.0]), Permeability parameter (K $\in$ [0.3, 1.0]), Powell-Eyring fluid parameter ($\lambda \in$ [0.3, 1.0]), Stretching sheet parameter (n $\in$ [0.3, 1.0]), Prandtl number (Pr $\in$ [0.71, 7.0]), and Lewis number (Le $\in$ [0.5, 1.8]).

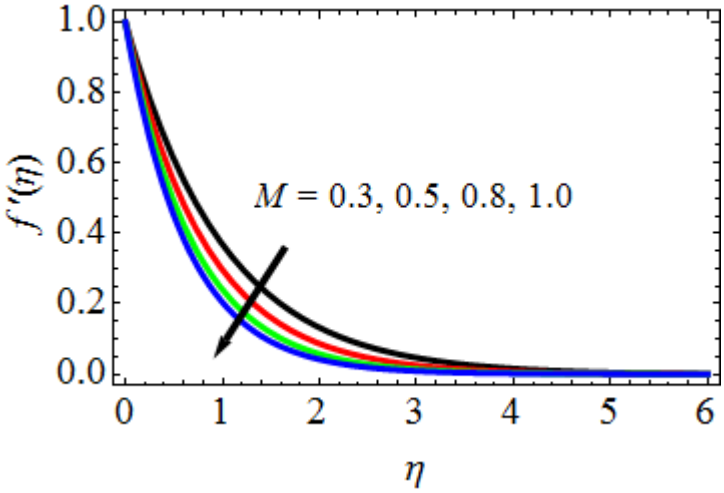

Fig. 3. Profiles of Velocity for variations of M

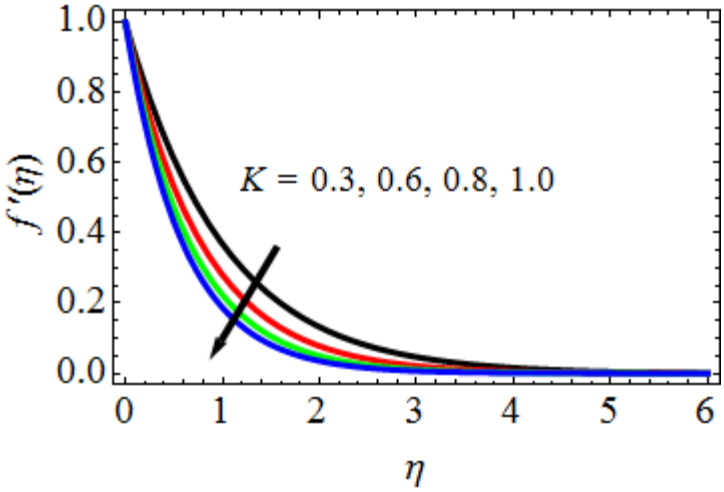

Fig. 4. Velocity Profiles for variations of K

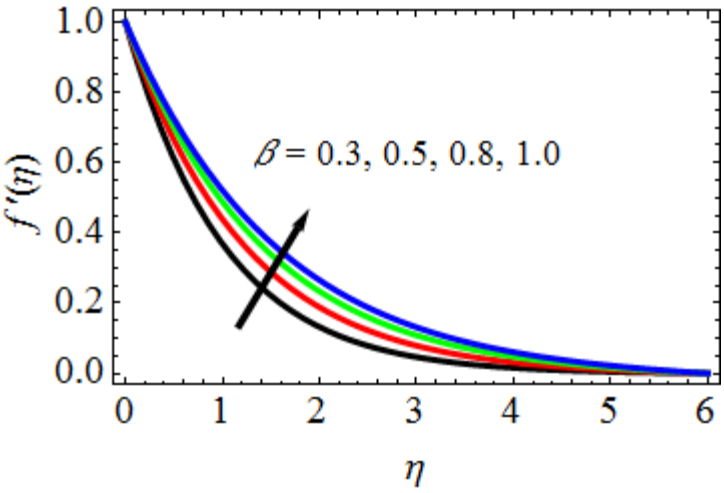

Fig. 5. Velocity Profiles for variations of β

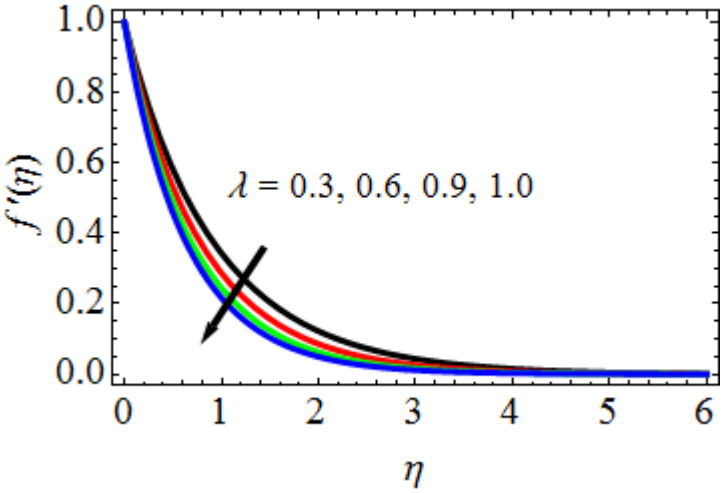

Fig. 6. Velocity Profiles for variations of λ

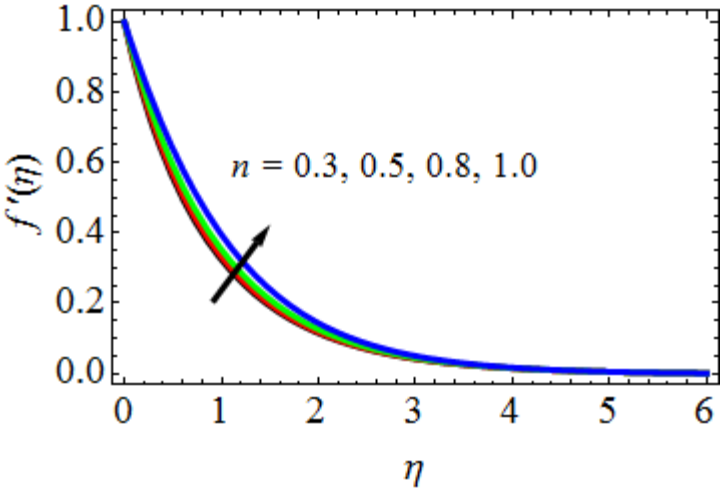

Fig. 7. Profiles of Velocity for variations of n

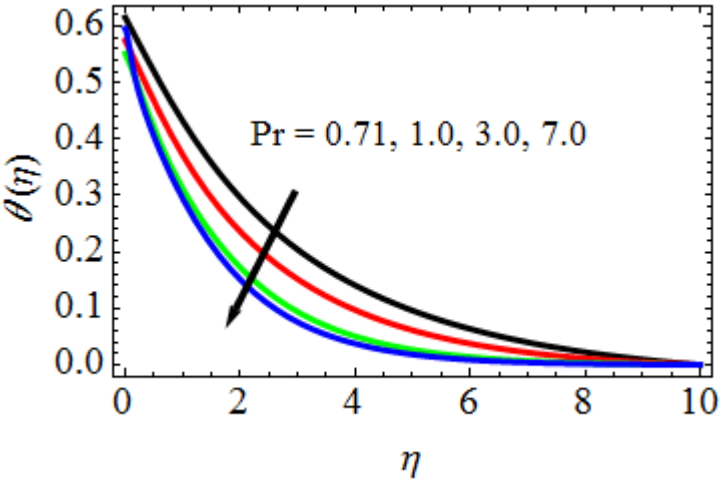

Fig. 8. Temperature profiles for variations of Pr

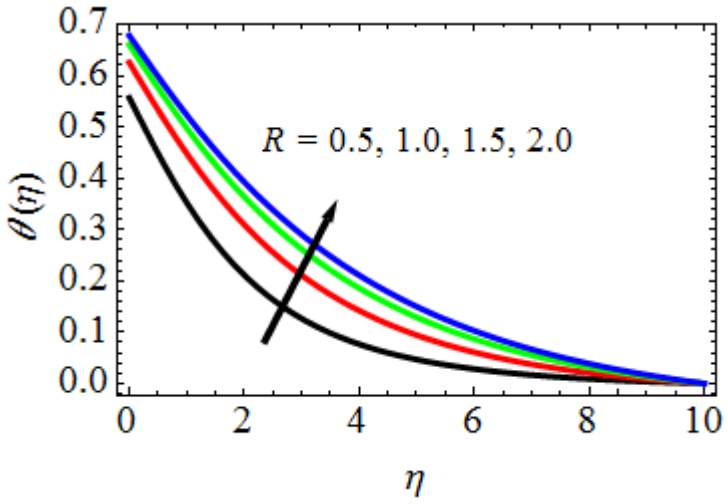

Fig. 9. Profiles of Temperature for variations of R

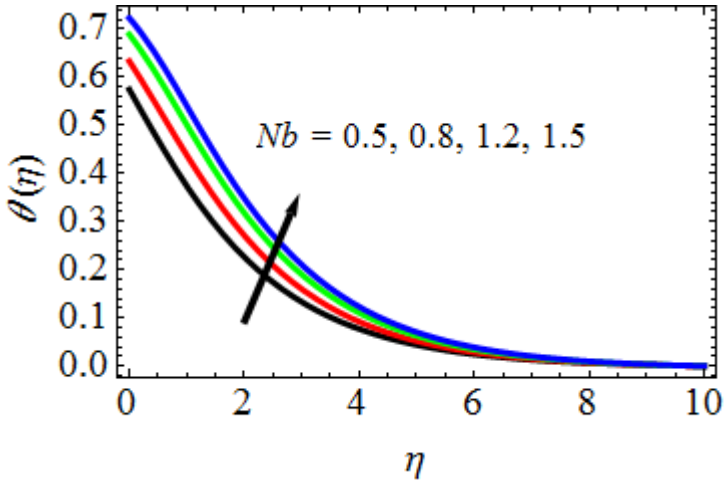

Fig. 10. Profiles of Temperature for variations of Nb

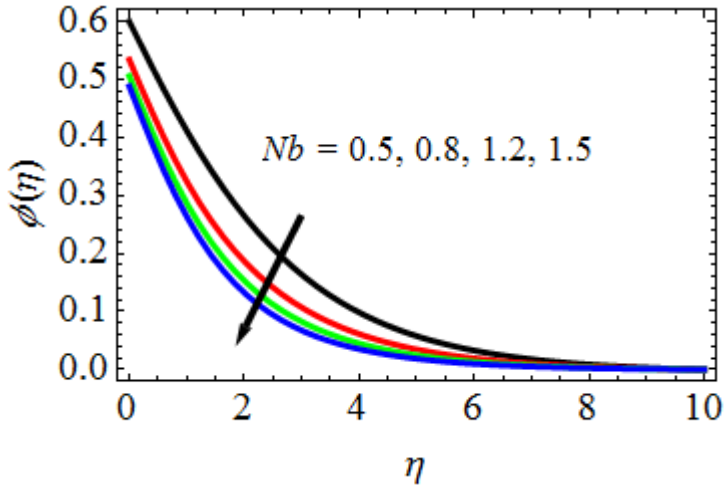

Fig. 11. Profiles of Concentration for variations of Nb

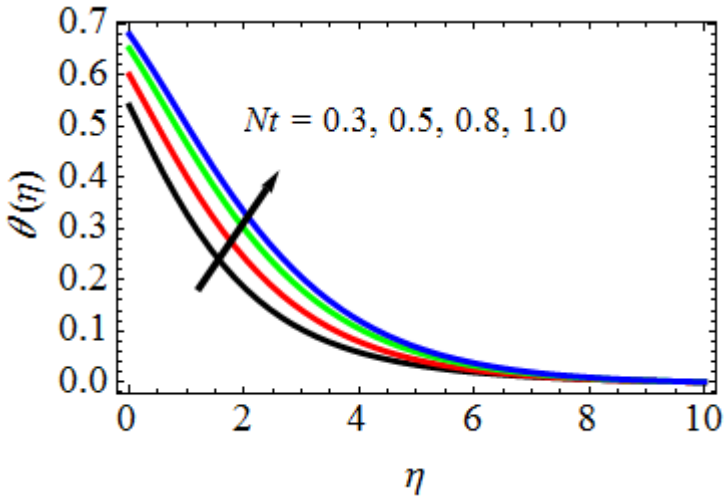

Fig. 12. Profiles of Concentration for variations of Nt

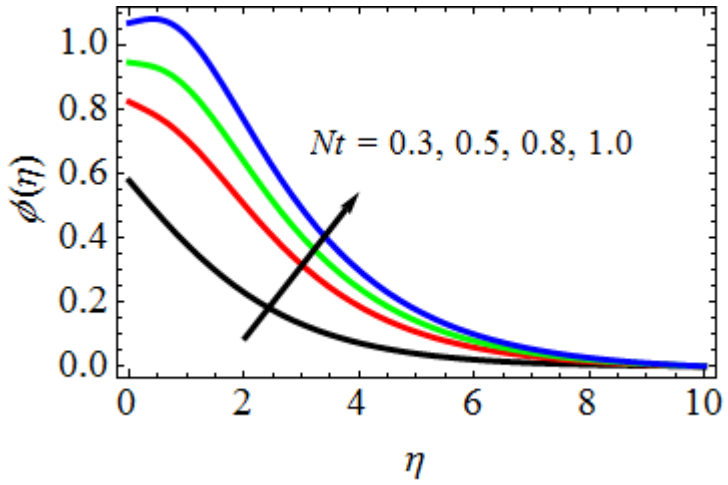

Fig. 13. Profiles of Concentration for variations of Nt

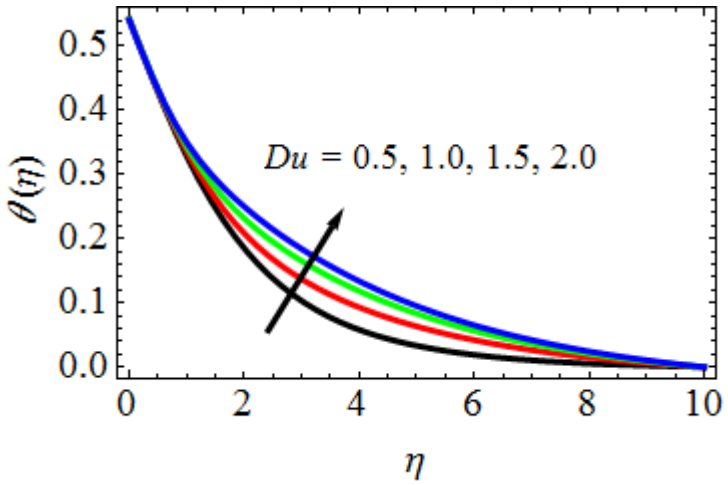

Fig. 14. Profiles of Concentration for variations of Du

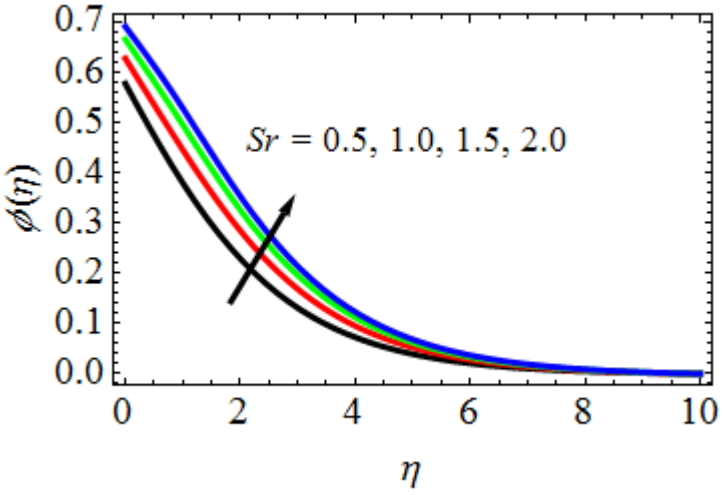

Fig. 15. Profiles of Concentration for variations of Sr

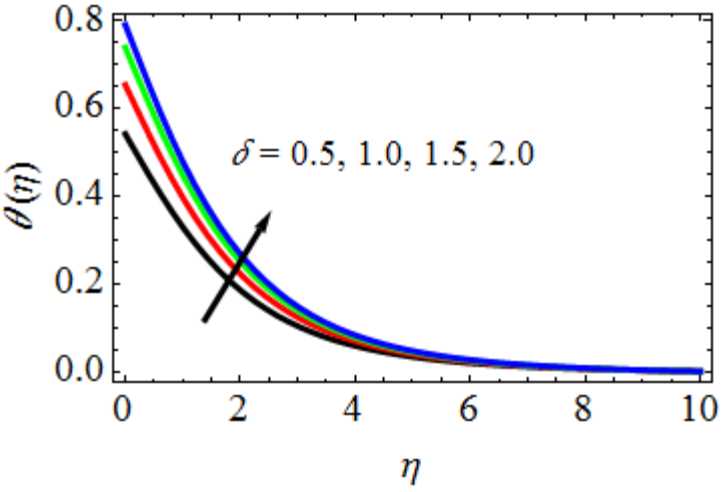

Fig. 16. Profiles of Temperature for variations of δ

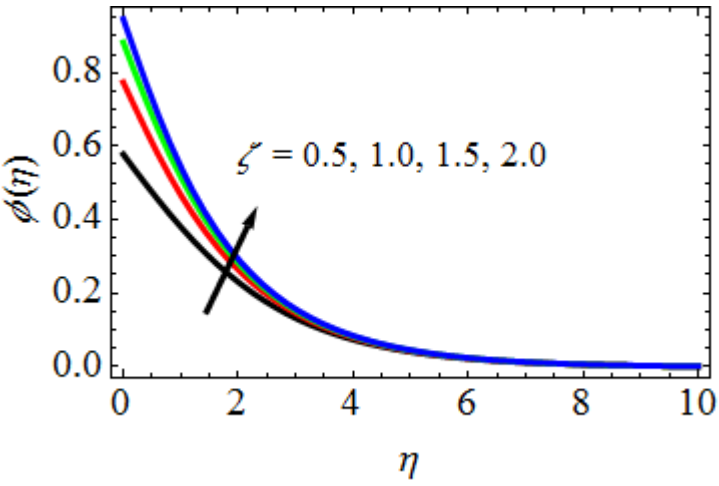

Fig. 17. Profiles of Concentration for variations of ζ

Table-2: Skin-friction coefficient values for different values of M, β, K, λ, n, Pr, Nb, Nt, Du, Sr, δ, ζ, Le and R in Numerical

M	β	K	λ	n	Pr	Nb	Nt	Du	Sr	δ	ζ	Le	R	Cf
0.3	0.3	0.3	0.3	0.3	0.71	0.5	0.3	0.5	0.5	0.5	0.5	0.5	0.5	1.355674780348467
0.5														1.315468741873473
0.8														1.292482859898549
	0.3													1.387186910986987
	0.5													1.408896017679833
		0.6												1.310878198679898
		0.8												1.289761907609866
			0.6											1.332734137340539
			0.9											1.315947134379008
				0.5										1.321527398278787
				0.8										1.307849898590122
					1.00									1.318698985813296
					3.00									1.298518133340738
						0.8								1.379877139487091
						1.2								1.397897391349339
							0.5							1.387882589896398
							0.8							1.398981936819083
								1.0						1.386784390843604
								1.5						1.406783934803981
									1.0					1.379676873904875
									1.5					1.398087834987302
										1.0				1.369574713487439
										1.5				1.379564174373464
											1.0			1.370798189346739
											1.5			1.387788848948195
												1.0		1.338678987190838
												1.5		1.317877327259005
													1.0	1.375741838457876
													1.5	1.386663889073439

Table-3: values in Numerical of coefficient of heat transfer rate for different values of Pr, Nb, Nt, Du, δ, and R

Pr	Nb	Nt	Du	δ	R	Nu
0.71	0.5	0.3	0.5	0.5	0.5	0.406643734857734
1.00						0.367758193876027
3.00						0.347414090654981

	0.8					0.431485238258938
	1.2					0.456781983896817
		0.5				0.447734093609373
		0.8				0.467881837490859
			1.0			0.456713793678990
			1.5			0.471178873437306
				1.0		0.437681893986981
				1.5		0.447851689375692
					1.0	0.437671736987316
					1.5	0.450981868163769

Table-4: values of coefficient rate of
mass transfer for various values of Nb, Nt, Sr, ζ, and Le in Numerical

Nb	Nt	Sr	ζ	Le	Sh
0.5	0.3	0.5	0.5	0.5	0.516733879369383
0.8					0.487784187906349
1.2					0.462156693194964
	0.5				0.537898478498198
	0.8				0.550983619836381
		1.0			0.530471836981929
		1.5			0.551886598398396
			1.0		0.531766137067309
			1.5		0.549787846730939
				1.0	0.487881983698960
				1.5	0.462567107373278

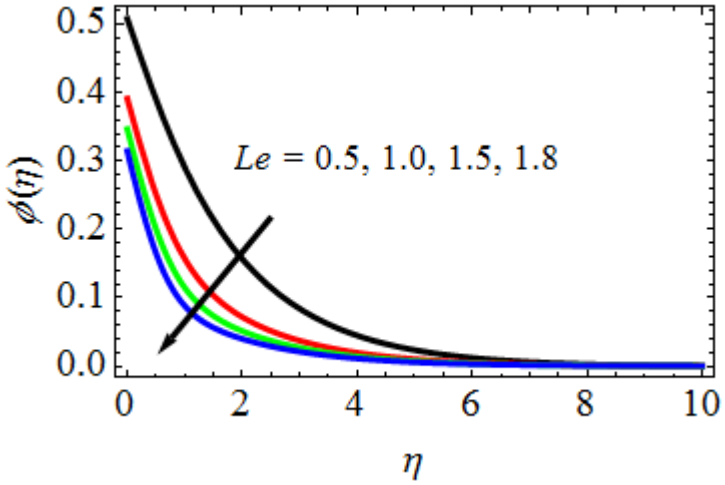

Fig. 18. profiles of Concentration for variations of Le

The values in numerical of Nusselt number or of coefficient rate of heat transfer are displayed in table-3 for various Prandtl number values (Pr ∈ [0.71, 7.0]), Thermal radiation parameter

(R∈ [0.5, 1.0]), parameter of Thermophoresis (Nt ∈ [0.3, 1.0]), parameter of Brownian motion (Nb ∈ [0.5, 1.5]), Diffusion thermo parameter or Dufour number (Du ∈ [0.5, 2.0]), and Thermal Biot number (δ ∈ [0.5, 2.0]). It is clear from this table that the coefficient of heat transfer rate is gradually rising with higher thermal radiation parameter values (R∈ [0.5, 1.0]), Parameter of Thermophoresis (Nt ∈ [0.3, 1.0]), parameter of Brownian motion Nb ∈ [0.5, 1.5]), Diffusion thermo parameter or Dufour number (Du ∈ [0.5, 2.0]), and Thermal Biot number (δ ∈ [0.5, 2.0]), while the overturn as the Prandtl Number (Pr ∈ [0.71, 7.0])increases so does the effect. The joint effects of Thermophoresis parameter (Nt ∈ [0.3, 1.0]), parameter of Brownian motion (Nb ∈ [0.5, 1.5]), Thermal diffusion parameter or Soret number (Sr ∈ [0.5, 2.0]), Mass Biot number (ζ ∈ [0.5, 2.0]) and Lewis number (Le ∈ [0.5, 1.8]) on mass transfer coefficient rate are analyzed in Table-4. From this table, it is viewed that the coefficient of mass transfer rate is growing with the parameter of Thermophoresis (Nt ∈ [0.3, 1.0]) increasing values. Thermal diffusion parameter or Soret number (Sr ∈ [0.5, 2.0]), Mass Biot number (ζ ∈ [0.5, 2.0]) and declining with incresing values of the parameter of Brownian motion (Nb ∈ [0.5, 1.5]), and Lewis number (Le ∈ [0.5, 1.8]).

6. Conclusions:

The flow that was examined in this study showed how, when a magnetic field is present and a porous material, Thermodynamic diffusion (Dufour) and diffusion thermo had an impact on the nanofluid Powell-Eyring flow past a stretched sheet. The basic flow model equations' similarity solution is obtained using combining the Runge-Kutta technique along with the shooting methodology. The key findings of this investigation are as follows:

- The profiles of velocity and thickness of momentum boundary decrease using the fluid parameters M, K and λ, while increase with n and β.
- Temperature profiles are improved with increasing R, Nb, Nt, Du, and falls with rising values of Pr.
- For large thermal Biot number δ, It was found that there was a sudden shift in the profiles of temperature.
- The boundary layer and the profiles of concentration both demonstrate a decline in concentration with Nb, Le and increase with Nt, Sr and ζ.
- Finally, the gained mathematical results are more accurate through the published results of Cortell [39] in a limiting case by taking $M \to 0$, $\beta \to 0$, $\lambda \to 0$, $K \to 0$, $Sr \to 0$, and $Du \to 0$.

According to the findings of this study, raising the value of fluid parameter will result the fluid to accelerate more quickly, and the random motion of the fluid will allow it to create more heat that may be used in industrial applications. Research in the future will take a two-pronged approach, looking in hybrid nanofluids at the dynamics of using Powell-Eyring type fluid heat transfer with convective boundary conditions as the basic fluid and investigating the behaviour of additional non-Newtonian fluid types (such as Casson, Ferro, Oldroyd B-fluid, Williamson fluids, etc.) behave under similar conditions. The fluid of Powell-Eyring type will be used as the base fluid for this research.

References:

1. Ali, H., & Rashidi, M. M. (2019). Experimental and numerical investigation of Powell-Eyring nanofluid flow and heat transfer in a concentric annulus. Powder Technology, 345, 152-163.
2. Aziz A, Asghar S, Uddin J, Numerical study of Powell-Eyring nanofluid flow over a stretching sheet. Journal of Molecular Liquids. 2019; 291: 111286.
3. Bachok N, Ishak A, Pop I. Unsteady MHD Powell-Eyring nanofluid flow over a stretching/shrinking sheet with heat source/sink. Journal of Molecular Liquids. 2019; 277: 730-737.
4. Bora G, Baruah DC, Sarma R. MHD Powell-Eyring nanofluid flow over a moving surface with thermal radiation and chemical reaction. Journal of Magnetism and Magnetic Materials. 2018; 460: 46-55.
5. Ghadimi, A., Rashidi, A. M., & Lorenzini, G. (2018). An experimental investigation of the flow of Powell-Eyring nanofluid in a rectangular microchannel. International Journal of Heat and Mass Transfer, 116, 1113-1122.
6. Ghadimi, A., Rashidi, A. M., & Lorenzini, G. (2019). Flow of Powell-Eyring nanofluid in a microchannel with a T-junction. Powder Technology, 342, 290-301.
7. Jamil M, Malik MY, Hussain A, Entropy generation analysis in Powell-Eyring nanofluid flow over a rotating disk with viscous dissipation. Journal of Molecular Liquids. 2021; 332: 115885.
8. Kamali, R., Noghrehabadi, A., & Jafari, A. (2020). Numerical study of turbulent Powell-Eyring nanofluid flow and heat transfer in a channel with a wall-mounted obstacle. International Journal of Heat and Mass Transfer, 149, 119179.
9. Karami, M., Rashidi, M. M., & Lorenzini, G. (2016). Numerical investigation of Powell-Eyring nanofluid flow and heat transfer in a rotating system. Powder Technology, 301, 592-602.
10. Karimipour, A., Rashidi, S., & Sheikholeslami, M. (2017). Magnetohydrodynamic Powell-Eyring nanofluid flow in a vertical channel with moving wall. Journal of Molecular Liquids, 238, 340-348.
11. Khodadadi, A., & Rashidi, M. M. (2018). Numerical analysis of Powell-Eyring nanofluid flow and heat transfer in a lid-driven square cavity. Powder Technology, 335, 252-265.
12. Li, J., Zhang, Y., Guo, L., & Wang, X. (2019). Theoretical study of the Powell-Eyring nanofluid flow in a microchannel. Journal of Applied Fluid Mechanics, 12(2), 411-419.
13. Liu, X., & Zhang, X. (2020). Investigation on the flow behavior of Powell-Eyring nanofluid in a curved microchannel. Heat Transfer Research, 51(13), 1209-1222.
14. Malik MY, Jamil M, Hussain A, Entropy analysis in Powell-Eyring nanofluid flow with thermal radiation and convective boundary conditions. Results in Physics. 2021; 22: 104091.
15. Mishra, R., & Mehta, K. N. (2018). Flow of Powell-Eyring nanofluid over a stretching sheet with convective boundary conditions. Journal of Heat Transfer, 140(6), 062501.
16. Nouri-Borujerdi, A., Mirzabeigy, A., Rashidi, A. M., & Zhang, Y. (2020). Experimental investigation and CFD simulation of heat transfer and fluid flow characteristics of Powell-Eyring nanofluid. Journal of Molecular Liquids, 309, 113055.
17. Oztop HF, Bhatti MM, Chamkha AJ. Nanofluid flow over a stretching sheet with convective boundary condition in the presence of thermal radiation. International Journal of Heat and Mass Transfer. 2017; 104: 428-435.
18. Rashidi, S., & Karimipour, A. (2016). Powell-Eyring nanofluid flow in a rotating curved channel with heat transfer analysis. Journal of Thermal Analysis and Calorimetry, 123(2), 1407-1418.
19. Rashidi, S., & Rashidi, M. M. (2016). Investigation of Powell-Eyring nanofluid flow and heat transfer in a channel partially filled with porous media. Powder Technology, 296, 130-142.

20. Rashidi, S., Karimipour, A., & Bovand, M. (2018). Powell-Eyring nanofluid flow in a vertical porous channel with magnetic field effect. Journal of Thermal Analysis and Calorimetry, 134(2), 1005-1016.
21. Rashidi, S., Karimipour, A., & Rashidi, M. M. (2017). Powell-Eyring nanofluid flow in a channel with a porous moving wall. Journal of Thermal Analysis and Calorimetry, 130(3), 2023-2033.
22. Rezaei M, Afrand M, Zeinali Heris S. A comprehensive review of Powell-Eyring nanofluid flow and heat transfer: Models and applications. Powder Technology. 2019; 357: 546-577.
23. Sahoo S, Satapathy AK, Mishra SR. Numerical analysis of Powell-Eyring nanofluid flow in a T-junction microchannel. Journal of Thermal Analysis and Calorimetry. 2019; 138: 2099-2109.
24. Sahoo S, Singh AK, Mishra SR, Satapathy AK. Numerical study of Powell-Eyring nanofluid flow in a rectangular microchannel. J. Thermal Analysis and Calorimetry, 2020; 139: 1183-1193.
25. Saqib, M., Hayat, T., & Alsaedi, A. (2017). Numerical simulation of Powell-Eyring nanofluid flow by means of Caputo-Fabrizio fractional derivative. Journal of Molecular Liquids, 241, 723-729.
26. Sattari, A., Hatami, M., Sheikholeslami, M., & Rashidi, S. (2021). Numerical study of mixed convection Powell-Eyring nanofluid flow in a lid-driven cavity. Powder Technology, 380, 104-115.
27. Seetharamu, K. N., & Sundararajan, T. (2015). Modeling and simulation of Powell-Eyring nanofluid flow through a pipe. International Journal of Heat and Mass Transfer, 80, 406-413.
28. Sharma A, Bhargava R. Powell-Eyring nanofluid flow and heat transfer: A review. Applied Thermal Engineering. 2019; 155: 631-644.
29. Sheikholeslami, M., & Rashidi, S. (2017). Numerical analysis of Powell-Eyring nanofluid flow and heat transfer in a cavity with wavy walls. Journal of Molecular Liquids, 232, 394-403.
30. Vafai, K., & Khaledi, K. (2018). Unsteady mixed convection flow of Powell-Eyring nanofluid in a vertical channel with asymmetric boundary conditions. International Journal of Heat and Mass Transfer, 117, 299-308.
31. Wang, L., & Pop, I. (2020). Numerical study of Powell-Eyring nanofluid flow over a permeable stretching surface. Journal of Nanofluids, 9(3), 604-612.
32. Wang, Y., Liu, Z., & Yang, X. (2017). Heat transfer and friction factor correlations for Powell-Eyring nanofluid in a circular tube under laminar flow conditions. International Journal of Heat and Mass Transfer, 107, 191-200.
33. Wong, K. V., & Leon, O. D. (2017). Heat transfer enhancement in Powell-Eyring nanofluids using single-walled carbon nanotubes. International Journal of Heat and Mass Transfer, 106, 1272-1280.
34. Wongwises, S., & Hayat, T. (Eds.). (2019). Powell-Eyring nanofluid dynamics. Springer.
35. Yu, H., Chen, J., Zhang, H., & Su, Y. (2019). Effect of thermal radiation on Powell-Eyring nanofluid flow in a channel with an expanding or contracting wall. International Journal of Heat and Mass Transfer, 128, 385-394.
36. Zaki, M., Ellahi, R., & Vafai, K. (2019). Convective heat transfer of Powell-Eyring nanofluid flow in a porous channel. Journal of Porous Media, 22(7), 813-824.
37. Zhang, Y., Li, J., Wang, X., & Chen, J. (2018). Flow of Powell-Eyring nanofluid in a T-shaped microchannel with expansion-contraction. International Journal of Heat and Mass Transfer, 120, 333-340.
38. Zheng, L., & Zheng, L. (2017). Powell-Eyring nanofluid flow and heat transfer over a stretching sheet. International Journal of Heat and Mass Transfer, 108, 75-84.
39. R. Cortell, Viscous flow and heat transfer over a nonlinearly stretching sheet, Appl. Math. Comput. 184 (2007) 864-873.